ACS APPLIED MATERIALS & INTERFACES

Research Article

www.acsami.org

Synthesis of Large-Area Highly Crystalline Monolayer Molybdenum Disulfide with Tunable Grain Size in a H_2 Atmosphere

Yulin Feng,[†] Kailiang Zhang,*[,†] Fang Wang,[†] Zhiwen Liu,[‡] Mingxu Fang,[†] Rongrong Cao,[†] Yinping Miao,[†] Zhengchun Yang,[†] Wei Mi,[†] Yemei Han,[†] Zhitang Song,[§] and H. S. Philip Wong*[,∥]

[†]School of Electronic Information Engineering, Tianjin Key Laboratory of Film Electronic & Communication Devices, Tianjin University of Technology, Tianjin, 300384, China

[‡]Keysight Technologies (China) Co., Ltd., Beijing, 100102, China

[§]State Key Laboratory of Functional Materials for Informatics, Shanghai Institute of Microsystem and Information Technology, Chinese Academy of Sciences, Shanghai, 200050, China

[∥]Department of Electrical Engineering and Center for Integrated Systems, Stanford University, Stanford, California 94305, United States

Supporting Information

ABSTRACT: Large-area and highly crystalline monolayer molybdenum disulfide (MoS_2) with a tunable grain size was synthesized in a H_2 atmosphere. The influence of introduced H_2 on MoS_2 growth and grain size, as well as the corresponding mechanism, was tentatively explored by controlling the H_2 flow rate. The as-grown monolayer MoS_2 displays excellent uniformity and high crystallinity evidenced by Raman and high-resolution transmission electron microscopy. The Raman results also give an indication that the quality of the monolayer MoS_2 synthesized in a H_2 atmosphere is comparable to that synthesized by using seed or mechanical exfoliation. In addition, the electronic properties and dielectric inhomogeneity of MoS_2 monolayers were also detected *in situ* via scanning microwave microscopy, with measurements on impedance and differential capacitance (dC/dV). Back-gated field-effect transistors based on highly crystalline monolayer MoS_2 shows a field-effect mobility of ~13.07 $cm^2\ V^{-1}\ s^{-1}$ and an I_{on}/I_{off} ratio of $\sim 1.1 \times 10^7$, indicating that the synthesis of large-area and high-quality monolayer MoS_2 with H_2 is a viable method for electronic and optoelectronic applications.

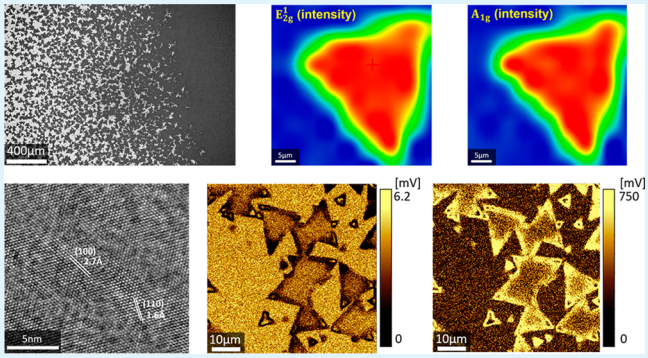

KEYWORDS: *molybdenum disulfide, highly crystalline, grain size, H_2, scanning microwave microscopy*

INTRODUCTION

Two-dimensional (2D) materials including graphene, boron nitride (BN), and transition-metal dichalcogenides (TMDs) have attracted considerable interest and been substantially researched, because of the intriguing electronic and optical properties, which are different between the monolayer crystal and the bulk form.[1−6] As one of the most potential materials in TMDs, molybdenum disulfide (MoS_2), a derivative of graphene, has gained significant research attention in recent years for electronic and optoelectronic applications.[3,5−9] Meanwhile, the preparation process of high-quality MoS_2 monolayers becomes more critical to achieve high-performance devices such as field-effect transistors (FETs) and sensors.[5,7−10] Much research on fabrication process has been made to improve the growth of the MoS_2 monolayers, such as scotch-tape-assisted micromechanical exfoliation,[1,5,11−13] liquid exfoliation,[14,15] chemical vapor deposition (CVD),[16−20] physical vapor deposition (PVD),[21] hydrothermal synthesis,[22] atomic layer deposition,[23] electrochemical synthesis,[24] thermolysis of compounds containing Mo and S sources,[25] and sulfurization of Mo oxides or Mo metal seed layers.[26−29]

In comparison with mechanical exfoliation, which offers a feasible way to obtain MoS_2 monolayers and other synthetic methods with limited quality and relatively complicated process, CVD has more advantages, such as the conformal, scalable, easily operational, and precisely controllable nature of highly crystalline MoS_2 monolayers grown on different substrates and domains.[17,19,20] Extensive investigations have been concentrated on the synthesis process and corresponding mechanism of CVD-MoS_2 with seed (such as perylene-3,4,9,10-tetracarboxylic dianhydride (PTCDA) and perylene-3,4,9,10-tetracarboxylic acid tetrapotassium (PTAS)),[8,16,17,30] Mo[26−28] or MoO_3 nanoribbons.[29] Considering the compatibility of MoS_2 with the subsequent processes and practical applica-

Received: July 31, 2015
Accepted: September 22, 2015
Published: September 22, 2015

DOI: 10.1021/acsami.5b07038
ACS Appl. Mater. Interfaces 2015, 7, 22587−22593

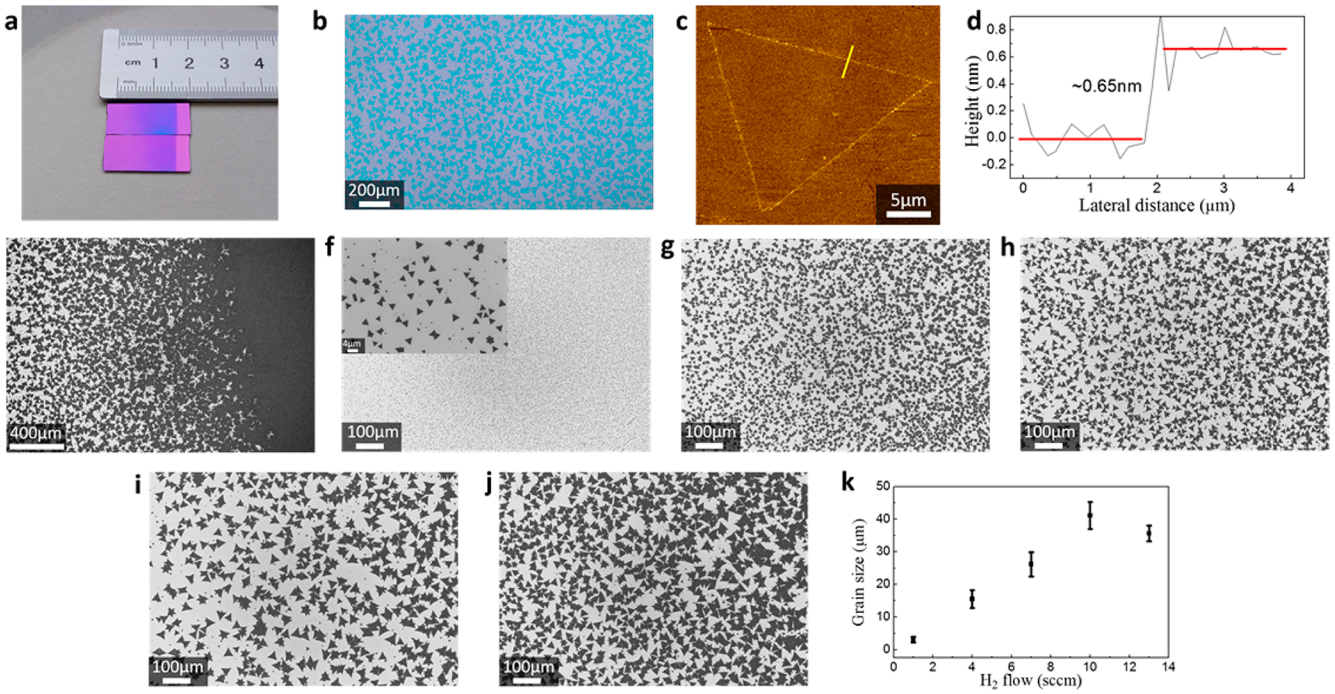

Figure 1. As-grown monolayer MoS_2: (a) photograph of the MoS_2 on SiO_2/Si substrates; (b) optical and (e) SEM images of the large area and uniform MoS_2 flakes; (c) AFM image also shows a synthesized uniform MoS_2 surface; (d) height profile of the MoS_2 flake indicated in panel (c), revealing that the MoS_2 is monolayer; (f–k) variation of monolayer MoS_2 grain size under different H_2 flow rates ((f) 1, (g) 4, (h) 7, (i) 10, and (j) 13 sccm); and (k) statistical results of grain size by measuring 100 MoS_2 triangular nanosheets under each condition.

tions,[31] the growth of large-area, uniform, and highly crystalline monolayer MoS_2 without substrate modifications and the corresponding reaction mechanism should be further investigated.

In this contribution, we synthesized large-area, uniform, and highly crystalline monolayer MoS_2 with MoO_3 and S at atmospheric pressure in H_2 atmosphere by using the CVD method. The influence of H_2 flow rate on MoS_2 grain size was investigated. Scanning microwave microscopy (SMM) was employed to measure the electronic properties and detect the dielectric inhomogeneity of the as-synthesized MoS_2 monolayers *in situ*. After characterization on the quality of the as-grown MoS_2, the electrical performance was evaluated by measuring the carrier mobilities and I_{on}/I_{off} ratios of the as-fabricated back-gated FETs.

RESULTS AND DISCUSSION

In this study, the MoS_2 monolayers were synthesized on SiO_2/Si substrates with high-purity MoO_3 and S as precursors, using a two-temperature-zone tube furnace (for details and a schematic diagram, see Figure S1 in the Supporting Information). Briefly, the substrates were treated with piranha solution (H_2SO_4/H_2O_2 = 3:1) followed by sonication in acetone and isopropanol (IPA) for 10 min before the growth. A quantity of 120 mg of MoO_3 was placed at Zone I of the furnace with substrates on the upper side, and 240 mg of S was located upstream in the low-temperature zone. After purging with 400 sccm Ar for 1 h at 100 °C, the flow was reduced to 80 sccm (Ar:H_2 = 7:1) at ambient pressure. The furnace temperature was gradually increased from 100 °C to 700 °C with a heating rate of 15 °C/min and the growth process was conducted at 700 °C for 10 min before being cooled to room temperature.

Influence of H_2 on MoS_2 Growth and Reaction Mechanism Analysis. Figures 1a, 1b, and 1e illustrate the uniform and large-area MoS_2 grown on SiO_2 substrates in a H_2 atmosphere. The MoS_2 monolayers with uniform contrast and triangular shape were observed in optical and scanning electron microscopy (SEM) images. The height of the triangular domain is confirmed by using atomic force microscopy (AFM) images (shown in Figures 1c and 1d), indicating that the MoS_2 was grown as a single layer. From the large area of the as-synthesized monolayer MoS_2, it can be concluded that the introduction of H_2 into the furnace can facilitate the nucleation of MoS_2 crystals on SiO_2 substrates, followed by extension to a two-dimensional (2D) nanosheet instead of crystals with packed MoS_2 layers (see Figure S2 in the Supporting Information). Here, the influence of introduced H_2 volume on the MoS_2 grain size was investigated in this study by controlling the H_2 flow rate during growth. As shown in Figures 1f–k, the grain size gradually increases as the H_2 flow rate increases from 1 sccm to 10 sccm and achieved a maximum value of ~41 μm. Generally, the reaction of S and MoO_3 in the vapor phase is described by eq 1, which can be further divided into two steps, as seen in eqs 2 and 3.[17,32]

$$2MoO_3 + 7S \rightarrow 2MoS_2 + 3SO_2 \quad (1)$$

$$MoO_3 + \frac{x}{2}S \rightarrow MoO_{3-x} + \frac{x}{2}SO_2 \quad (2)$$

$$MoO_{3-x} + \frac{(7-x)}{2}S \rightarrow MoS_2 + \frac{(3-x)}{2}SO_2 \quad (3)$$

However, it is difficult for MoO_3 to react directly with S to form MoS_2 flakes. An intermediate state of MoO_3 is needed to achieve the transition to MoS_2 more efficiently. According to eqs 2 and 3, the MoO_3 is first turned to MoO_{3-x} by the reduction of S, followed by further sulfurization to form MoS_2.

DOI: 10.1021/acsami.5b07038
ACS Appl. Mater. Interfaces 2015, 7, 22587–22593

The concentration of the as-produced intermediate MoO_{3-x} determines the nucleation formation and growth efficiency of the MoS_2 from nucleation site to 2D nanosheet. Once a fraction of H_2 is introduced into the tube, the reaction of eq 4 would happen.

$$MoO_3 + xH_2 \rightarrow MoO_{3-x} + xH_2O \quad (4)$$

Based on eq 4, the introduced H_2, as a reducing agent and catalyst, would make the MoO_3 much easier to be converted to MoO_{3-x}, as well as be translated from Mo^{6+} to Mo^{4+}, which will increase the concentration of MoO_{3-x} that can react directly with S to form MoS_2 crystals. Consequently, the reaction efficiency is improved.[33−35] Meanwhile, the H_2S generated during growth will also react with MoO_{3-x} to synthesize MoS_2 monolayers (see eq 5):[32]

$$MoO_{3-x} + (1-x)H_2 + 2H_2S \rightarrow MoS_2 + (3-x)H_2O \quad (5)$$

Consequently, the reaction progress is improved. However, the grain size of MoS_2 decreases when the H_2 flow rate was further increased to 13 sccm, which might be caused by the further reduction reaction of MoO_{3-x} to Mo, reducing the synthesis efficiency, making the size of MoS_2 monolayers smaller than that growed with 10 sccm. The Raman and photoluminescence (PL) spectra of MoS_2 synthesized under different H_2 flow rates were obtained to evaluate the quality of flakes. As seen in Figure S3 in the Supporting Information, the peak positions and intensities in Raman spectra are almost the same and the PL spectra show a bandgap varing between 1.8 and 1.84 eV in synthesized MoS_2, revealing that the as-grown MoS_2 is a monolayer, with no significant difference in quality.[36] In addition, based on the optimal H_2 flow rate, the MoS_2 monolayers were also synthesized with different time (see Figure S4 in the Supporting Information). With longer growth time, the MoS_2 grain size can reach ~260 μm and can also form the large-area uniform monolayers, indicating the feasibility of monolayer MoS_2 synthesized using H_2. In addition, the as-grown MoS_2 monolayer reveals an atomically flat surface at the subnanometer level (see Figure S5 in the Supporting Information), indicating the introduced H_2 is beneficial to the horizontal growth and the uniformity of the synthesized MoS_2 monolayers.

Characterization on MoS_2 Microstructure and Uniformity. To further verify the layer number and analyze the crystal quality of the synthesized MoS_2 monolayers, Raman spectroscopy was performed. As shown in Figure 2a, two typical Raman active modes were obtained, centered at 401.1 cm^{-1} (A_{1g}) and 380.8 cm^{-1} (E^1_{2g}), which are associated with the out-of-plane vibration of S atoms and the in-plane vibration of Mo and S atoms, respectively (shown inset in Figure 2a). The frequency difference (Δ) value between the two peaks was ~20.3 cm^{-1}, indicating that the monolayer MoS_2 was achieved, which is in agreement with the results shown in Figure 1 and previous reports.[19,20,27,36,37] The intensity ratio of E^1_{2g}, relative to the substrate, was calculated to be 0.057, which corresponds to the MoS_2 single layer.[27] The typical Raman shifts of the synthesized MoS_2 monolayers in this study were also compared with that synthesized using seed and mechanical exfoliation, as represented in Figure 2b. The similar intensity and centered positions give a strong evidence that the quality of the two monolayer MoS_2 samples grown with different methods are comparable, which indicates the introduction of H_2 can improve the growth as well as quality of MoS_2 monolayers.

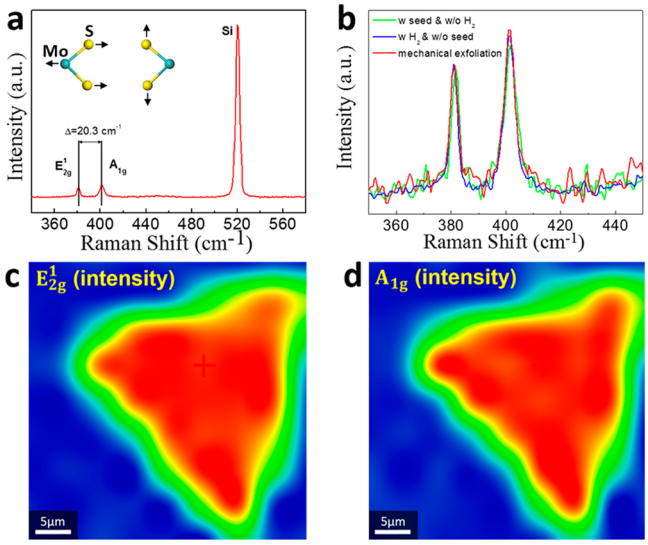

Figure 2. Raman spectra of the as-grown monolayer MoS_2: (a) Raman spectra with two active modes (E^1_{2g} and A_{1g}) of monolayer MoS_2 (the frequency difference is ~20.3 cm^{-1}); (b) comparison of the Raman spectra of monolayer MoS_2 synthesized with H_2 and with seed as well as mechanical exfoliation (the similar position and intensity reveal that the crystalline structure of the two samples is comparable). (c, d) Intensity of Raman mapping of E^1_{2g} (panel c) and A_{1g} (panel d), the contrast between monolayer MoS_2 and SiO_2 substrates reveals the uniformity of the MoS_2 monolayers grown in a H_2 atmosphere.

Moreover, the Raman mapping was performed to evaluate the uniformity of the MoS_2 monolayers. Figures 2c and 2d present the Raman intensity mapping with a total of 81 (9 × 9) Raman spectra collected from this domain. The peak positions of A_{1g} (401.1 cm^{-1}) and E^1_{2g} (380.8 cm^{-1}) were selected as the reference Raman shifts to highlight the different intensity of the mapping and to distinguish the MoS_2 crystal from SiO_2 substrates. Both mappings show the similar profile with the identical contrast in MoS_2 monolayer, manifesting the uniformity of the synthesized MoS_2.[27] Meanwhile, the relatively large step size (5 μm) with small spot size also has an impact on the mapping quality and MoS_2 domain uniformity. Nonetheless, the Raman spectra and mapping give strong evidence of the excellent uniformity and crystallinity of the monolayer MoS_2.

Transmission electron microscopy (TEM) was carried out to further elucidate the crystalline structure of the synthesized monolayer MoS_2. Figure 3a shows the morphology of MoS_2 monolayers covering on Cu grid with a rolled-up edge and wrinkles on the surface, which might be caused by the liquid transfer process. The area in the white dashed square was expanded to observe the atomic distribution. The hexagonal lattice structure is clearly observed in Figure 3b, and the Mo and S atoms are indicated in the image, which is the basic atomic arrangement of MoS_2, suggesting that the monolayer MoS_2 is highly crystallized. The high-resolution TEM (HRTEM) image (Figure 3c) and the corresponding selected area electron diffraction (SAED, Figure 3d) also reveal the hexagonal structure with the specific interplanar distances of 1.6 and 2.7 Å assigned to the (110) and (100) planes, respectively. The SAED pattern of the flake shows the diffraction spots of MoS_2 (110) and (100), as well as their equivalent planes, which corresponds to the planes observed in the HRTEM image,

DOI: 10.1021/acsami.5b07038
ACS Appl. Mater. Interfaces 2015, 7, 22587−22593

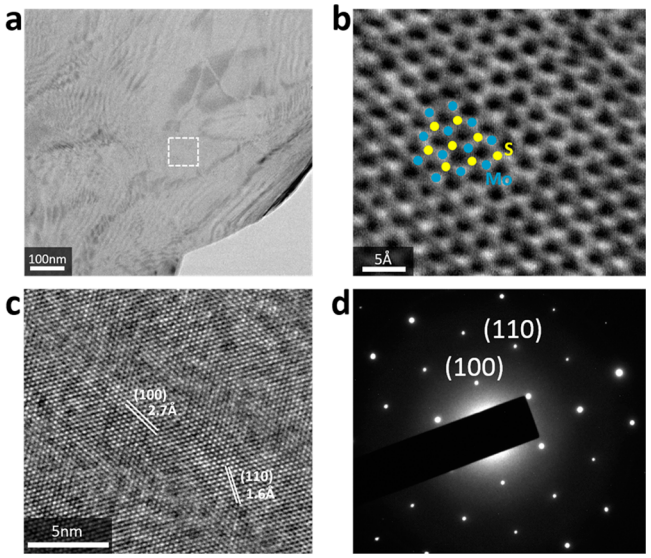

Figure 3. TEM images of the synthesized monolayer MoS_2: (a) the MoS_2 was transferred by liquid etching process with some rolled-up edges and wrinkles; (b) the hexagonal crystal structure of MoS_2 (the Mo atoms have much higher contrast than the S atoms, because of the atomic mass); (c) the HRTEM image shows the well-crystallized MoS_2 (the lattice spacing of 2.7 and 1.6 Å comes from the MoS_2 (100) and (110) planes); (d) in the SAED pattern, the bright diffraction spots indicate that the measured area in the sample is single crystal.

indicating that the selected area in the monolayer MoS_2 is single crystal.

The X-ray photoelectron spectrometry (XPS) system was also performed to characterize the monolayer MoS_2 crystal lattice structure and to investigate the elemental composition and chemical state of the MoS_2 monolayer with a power beam that can penetrate deeply in the sample. The detailed binding energy profiles are presented in Figure 4. The Mo 3d shows

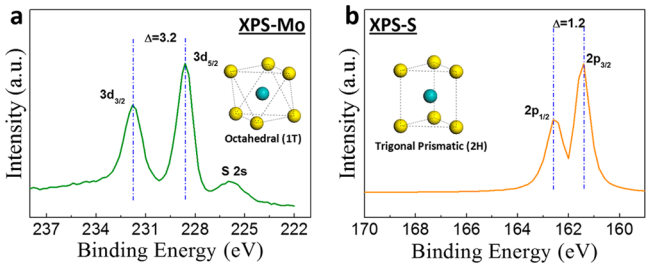

Figure 4. XPS was used to analyze the binding energy of the (a) Mo and (b) S atoms in the synthesized monolayer MoS_2. The structure of 2H-MoS_2 and 1T-MoS_2 was shown inset in the images.

two peaks at 228.6 and 231.8 eV, which are attributed to the doublet of Mo $3d_{5/2}$ and Mo $3d_{3/2}$, respectively. The peaks at 161.4 and 162.6 eV correspond to the S $2p_{3/2}$ and S $2p_{1/2}$ orbital of divalent sulfide ions, respectively. The Mo 3d spectra at ~229 and 232 eV are assigned to 2H-MoS_2 (structures are shown inset in Figure 4), which demonstrates a thermodynamically stable phase of MoS_2 existed in synthesized monolayer instead of a metastable phase (1T-MoS_2).[38,39] Note that the absence of prominent peaks at ~236 eV (corresponding to Mo^{6+} $3d_{5/2}$) illustrates the complete sulfurization of Mo atoms. The more MoO_3 is sulfurized, the fewer trap centers are induced by unreacted MoO_3 or unsaturated bonds, which can improve the reliability of the device based on MoS_2. Meanwhile, the stoichiometry of the MoS_2 monolayer deduced by XPS is also confirmed (S/Mo ≈ 2.03).

Measurement on Electronic Properties of Monolayer MoS_2. In order to evaluate the electrical performance of the as-grown monolayer MoS_2, the back-gated transistors with transferred MoS_2 samples were fabricated. Figures 5a–c show the typical transfer, and output characteristics of the device are shown in the inset in Figure 5b. The results indicate that the device is an *n*-type channel, which is in agreement with the previous reports.[5,7,29,30] From Figure 5a, the field-effect mobility of ~13.07 $cm^2\ V^{-1}\ s^{-1}$ can be extracted by using the expression $\mu = [dI_{ds}/dV_{ds}] \times [L/(WC_iV_{ds})]$, where L is the channel length and W is the channel width. C_i is the capacitance between the channel and the back gate per unit area, and the I_{on}/I_{off} ratio of ~1.18×10^7 can also be deduced by using a semilogarithmic coordinate in the inset shown in Figure 5a. Both the carrier mobility and the I_{on}/I_{off} ratio are comparable with the mechanically exfoliated or CVD-grown monolayer MoS_2 measured under the same conditions (ambient conditions, room temperature, and without high-*k* coatings),[7−9,29,30,36] which demonstrates the high quality of the MoS_2 that is achieved in a H_2 atmosphere. The device also exhibited excellent ohmic contacts (the contact resistance (R_c) was also measured by using the transfer length method (TLM) with channel lengths of 500 nm, 1 μm, and 2 μm; the results are shown in Figure S6 in the Supporting Information) at low V_{ds} (Figure 5b) and had a tendency to saturate at high V_{ds} (Figure 5c). In addition, a statistical distribution of the carrier mobility and the I_{on}/I_{off} ratio measured from 20 FETs made with monolayer MoS_2 are shown in Figure 5d. Generally, some defects, such as the vacancies and grain boundaries in the as-grown MoS_2, have a great impact on the performances of the device, resulting in small carrier mobility and performance nonuniformity from device to device. Therefore, the relatively uniform distributions shown in Figure 5 indicate the quality uniformity of the synthesized MoS_2 in the experiments and the less-polluted process of transfer and device fabrication.

On the other hand, to nondestructively detect the electronic properties and the nanoscale dielectric inhomogeneity of synthesized monolayer MoS_2 *in situ*, SMM was conducted to measure the impedance and the differential capacitance (dC/dV) of the flakes.[40] The microwave signal generated by the PNA is transmitted via a coaxial cable to a conductive AFM tip. By comparing the incident RF signal to the back-reflected signal, the magnitude and phase of the ratio are calculated. The capacitance coupling of probe-sample and a microwave signal with a few GHz, combined with the conductive AFM tip, enable the test to be performed without a dedicated electrode and has a high spatial resolution of ~30 nm. The frequency in this study for monolayer MoS_2 test was chosen at 7.26 GHz (more distinct signals can be achieved). Figure 6a shows the topography of the area with monolayer MoS_2, and the corresponding dC/dV amplitude and phase images are shown in Figures 6b and 6c, respectively. We can clearly observe the obvious contrasts in the two images, which might be ascribed to the different properties of the SiO_2 substrate (insulator) and monolayer MoS_2 (semiconductor). The sharpest transition between the substrates and the MoS_2 monolayer was seen in the dC/dV images, which results from the nanosized AFM tips. The impedance composed of PNA amplitude and phase was also measured, which corresponds to the capacitance and conductance of the MoS_2 monolayer (shown in Figures 6d and

DOI: 10.1021/acsami.5b07038
ACS Appl. Mater. Interfaces 2015, 7, 22587−22593

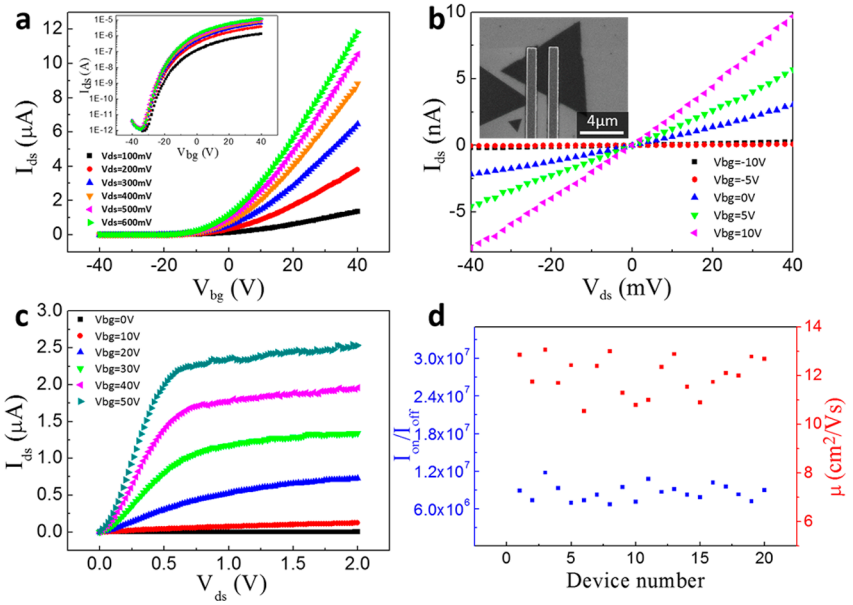

Figure 5. Electrical properties of monolayer MoS_2: (a) typical transfer characteristics (I_{ds}−V_{bg}) of the MoS_2 FETs with linear scale (inset is shown with a semilogarithmic scale); (b, c) typical output characteristics (I_{ds}−V_{ds}) of the MoS_2 FETs (inset shows the complete device measured for this figure with the best performance); and (d) statistical results of the field-effect mobilities (right *y*-axis) and I_{on}/I_{off} ratios (left *y*-axis) of 20 MoS_2 FETs.

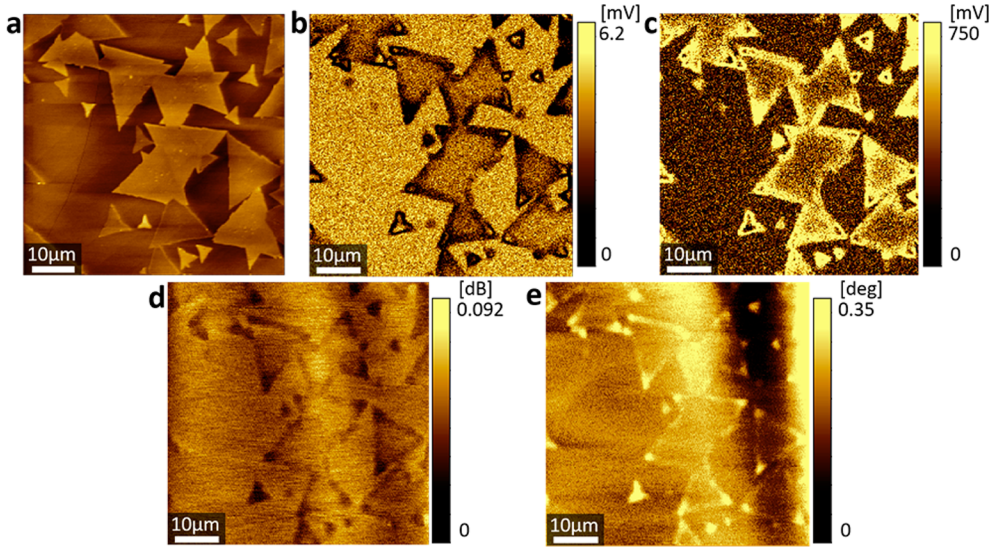

Figure 6. SMM results of monolayer MoS_2: (a) topography of monolayer MoS_2; (b) d*C*/d*V* amplitude image; (c) d*C*/d*V* phase image; (d) PNA amplitude image; and (e) PNA phase image. Stronger signals in all results are observed, which may be caused by measurement environments and the modules/cables used for RF generation and transmission. Some uncertain factors appear in the PNA amplitude and phase images, which should be further optimized with the configuration of the SMM system.

6e).[41,42] Unlike d*C*/d*V*, the signals of monolayer MoS_2 on PNA amplitude and phase were relatively weak, which corresponds to the lower impedance that originated from the intrinsic doping characteristics, as evidenced by the MoS_2-based field-effect transistors.[5,7,36] Moreover, a localized change in electronic inhomogeneity between the MoS_2 surface and the edges can be clearly observed in preliminary SMM measurements for both impedance and d*C*/d*V* images. This can be attributed to the dangling bonds on the edge of the 2D layered materials, leading to more contaminations and adsorbates. The intrinsic properties including the polarity of majority carriers and dopant level of the as-grown monolayer MoS_2 become more uniform in the MoS_2 plane, whereas a significant difference was observed at the boundaries. However, this phenomenon cannot be resolved by SEM (Figure 1) or AFM (Figure 6a), which indicates the superiority of the SMM on electronic inhomogeneity for 2D nanomaterials and also proves the capacity to detect such atomically thin 2D semiconductors.[43] Further understanding of the images to quantitatively calculate the parameters including dielectric constant and capacitance requiring finite-element analysis of the tip−sample interaction, will also be analyzed and reported in other reports.

CONCLUSION

In conclusion, we demonstrate the synthesis of large-area highly crystalline MoS_2 monolayer in a H_2 atmosphere. The grain size of MoS_2 first increases then decreases as the H_2 flow rate

DOI: 10.1021/acsami.5b07038
ACS Appl. Mater. Interfaces 2015, 7, 22587−22593

increases from 1 sccm to 13 sccm, and can reach ~260 μm when growth is performed using a H_2 flow rate of 10 sccm with longer growth time. The results characterized by AFM, SEM, Raman spectroscopy, XPS, and HRTEM reveal that the synthesized MoS_2 monolayer has excellent uniformity and high crystallinity. The electronic properties and the dielectric inhomogeneity of the as-grown MoS_2 monolayer was *in situ* measured by SMM, illustrating the different properties between the monolayer MoS_2 and substrates, as well as the different properties between the edge and the surface. The electrical performances of ~13.07 $cm^2 V^{-1} s^{-1}$ and the I_{on}/I_{off} of ~1.18×10^7 was obtained by measuring back-gated monolayer MoS_2 FETs under ambient conditions. This work suggests that synthesis in a H_2 atmosphere is a feasible and convenient way to achieve large-area and highly crystalline MoS_2 monolayers.

EXPERIMENTAL SECTION

Characterization of Monolayer MoS_2. The surface topography of MoS_2 monolayer was observed using optical microscopy (OM) (Nikon, Model LV150N), scanning electron microscopy (SEM) (Hitachi, Model S4800), and atomic force microscopy (AFM) (Agilent, Model 5600LS). Raman spectra and mapping were obtained by confocal Raman microscopy (ThermoFisher, Model DXR) at a laser power of 2 mW, an excitation wavelength of 532 nm, and a spot size of 1.2 μm, in which the Si peak at 520 cm^{-1} was used as a reference for wavenumber calibration. Photoluminescence (PL) (Witec, Model Alpha 300R) was conducted with a wavelength of 532 nm at a laser power of 1 mW. X-ray photoelectron spectroscopy (XPS) (PHI, Model 5000) was performed with monochromatic Al Kα X-ray source to determine the chemical configurations of the MoS_2. The electron analyzer was positioned at a fixed angle of 45° and the energy calibrations were made against the C 1s peak to eliminate the charging of the sample during analysis. Field-effect transmission electron microscopy (TEM) (FEI, Model Tecnai G2 T20) was applied at 200 keV to confirm the atomic structure of the MoS_2 monolayers. The as-grown MoS_2 monolayer was transferred onto a Cu grid by etching away the SiO_2 with a diluted hydrofluoric acid solution for TEM characterizations. A system composed of an AFM device and a two-port vector network analysis (VNA) device (Keysight, Model PNA-X N5244A) was used for scanning microwave microscopy (SMM).

Device Fabrication and Measurements. The devices were fabricated using e-beam lithography (EBL, Raith e_LINE plus). PMMA (4.2% 950 K) was spin-coated at 6000 rpm on SiO_2/Si with transferred samples using the same method described above. After lithography and development, 20 nm of Ti and 200 nm of Au were deposited as the electrodes using e-beam evaporation and magnetron sputtering, respectively. The samples were annealed in an Ar/H_2 (200/10 sccm) atmosphere at 200 °C for 2 h to improve the contact of the MoS_2 and metal. Electrical measurements were performed with a semiconductor parameter analyzer (Agilent, Model B1500A) under ambient conditions in a probe station (JANIS, Model ST-500).

ASSOCIATED CONTENT

Supporting Information

The Supporting Information is available free of charge on the ACS Publications website at DOI: 10.1021/acsami.5b07038.

Additional description of growth procedures of highly crystalline MoS_2, atomic force microscopy (AFM) images, scanning electron microscopy (SEM) images, root-mean-square (RMS) roughness, and Raman characterization as well as photoluminescence (PL) spectra (PDF)

AUTHOR INFORMATION

Corresponding Authors

*E-mail: kailiang_zhang@163.com.
*E-mail: hspwong@stanford.edu.

Author Contributions

K.Z. conceived the idea and designed the experiments. Y.F., F.W., M.F., R.C., and Z.Y. synthesized the MoS_2. Y.F., K.Z., Y.M., W.M., and Y.H. carried out the AFM, SEM, Raman, PL, TEM, and XPS characterizations. Y.F., K.Z., and Z.L. performed the SMM measurements. Y.F. fabricated the devices and measured the electrical performance of the monolayer MoS_2-based field-effect transistors. Y.F., K.Z., Z.S., and H.P.W. analyzed the data and wrote the manuscript.

Notes

The authors declare no competing financial interest.

ACKNOWLEDGMENTS

This work is supported by the National Natural Science Foundation of China (Grant Nos. 61274113, 11204212, and 61404091), and Program for New Century Excellent Talents in University (Grant No. NCET-11-1064), and Tianjin Natural Science Foundation (Grant Nos. 13JCYBJC15700, 13JCZDJC26100, 14JCZDJC31500, and 14JCQNJC00800), and Tianjin Science and Technology Developmental Funds of Universities and Colleges (Grant Nos. 20100703, 20130701, and20130702).

REFERENCES

(1) Novoselov, K. S.; Geim, A. K.; Morozov, S. V.; Jiang, D.; Zhang, Y.; Dubonos, S. V.; Grigorieva, I. V.; Firsov, A. A. Electric Field Effect in Atomically Thin Carbon Films. *Science* **2004**, *306*, 666−669.

(2) Geim, A. K.; Novoselov, K. S. The Rise of Graphene. *Nat. Mater.* **2007**, *6*, 183−191.

(3) Butler, S. Z.; Hollen, S. M.; Cao, L. Y.; Cui, Y.; Gupta, J. A.; Gutierrez, H. R.; Heinz, T. F.; Hong, S. S.; Huang, J. X.; Ismach, A. F.; Johnston-Halperin, E.; Kuno, M.; Plashnitsa, V. V.; Robinson, R. D.; Ruoff, R. S.; Salahuddin, S.; Shan, J.; Shi, L.; Spencer, M. G.; Terrones, M.; Windl, W.; Goldberger, J. E. Progress, Challenges, and Opportunities in Two-Dimensional Materials Beyond Graphene. *ACS Nano* **2013**, *7*, 2898−2926.

(4) Lee, K. H.; Shin, H.-J.; Lee, J. Y.; Lee, I. Y.; Kim, G.-H.; Choi, J.-Y.; Kim, S.-W. Large-Scale Synthesis of High-Quality Hexagonal Boron Nitride Nanosheets for Large-Area Graphene Electronics. *Nano Lett.* **2012**, *12*, 714−718.

(5) Radisavljevic, B.; Radenovic, A.; Brivio, J.; Giacometti, V.; Kis, A. Single-Layer MoS_2 Transistors. *Nat. Nanotechnol.* **2011**, *6*, 147−150.

(6) Wang, Q. H.; Kalantar-Zadeh, K.; Kis, A.; Coleman, J. N.; Strano, M. S. Electronics and Optoelectronics of Two-Dimensional Transition Metal Dichalcogenides. *Nat. Nanotechnol.* **2012**, *7*, 699−712.

(7) Liu, B. L.; Chen, L.; Liu, G.; Abbas, A. N.; Fathi, M.; Zhou, C. W. High-Performance Chemical Sensing Using Schottky-Contacted Chemical Vapor Deposition Grown Monolayer MoS_2 Transistors. *ACS Nano* **2014**, *8*, 5304−5314.

(8) Lee, Y.-H.; Yu, L. L.; Wang, H.; Fang, W. J.; Ling, X.; Shi, Y. M.; Lin, C.-T.; Huang, J.-K.; Chang, M.-T.; Chang, C.-S.; Dresselhaus, M.; Palacios, T.; Li, L. J.; Kong, J. Synthesis and Transfer of Single-Layer

DOI: 10.1021/acsami.5b07038
ACS Appl. Mater. Interfaces 2015, 7, 22587−22593

Transition Metal Disulfides on Diverse Surfaces. *Nano Lett.* **2013**, *13*, 1852−1857.
(9) Lopez-Sanchez, O.; Lembke, D.; Kayci, M.; Radenovic, A.; Kis, A. Ultrasensitive Photodetectors Based on Monolayer MoS_2. *Nat. Nanotechnol.* **2013**, *8*, 497−501.
(10) Perkins, F. K.; Friedman, A. L.; Cobas, E.; Campbell, P. M.; Jernigan, G. G.; Jonker, B. T. Chemical Vapor Sensing with Monolayer MoS_2. *Nano Lett.* **2013**, *13*, 668−673.
(11) Lembke, D.; Allain, A.; Kis, A. Thickness-Dependent Mobility in Two-Dimensional MoS_2 Transistors. *Nanoscale* **2015**, *7*, 6255−6260.
(12) Zou, X. M.; Wang, J. L.; Chiu, C.-H.; Wu, Y.; Xiao, X. H.; Jiang, C. Z.; Wu, W.-W.; Mai, L. Q.; Chen, T. S.; Li, J. C.; Ho, J. C.; Liao, L. Interface Engineering for High-Performance Top-Gated MoS_2 Field-Effect Transistors. *Adv. Mater.* **2014**, *26*, 6255−6261.
(13) Son, Y. W.; Wang, Q. H.; Paulson, J. A.; Shih, C.-J.; Rajan, A. G.; Tvrdy, K.; Kim, S.; Alfeeli, B.; Braatz, R. D.; Strano, M. S. Layer Number Dependence of MoS_2 Photoconductivity Using Photocurrent Spectral Atomic Force Microscopic Imaging. *ACS Nano* **2015**, *9*, 2843−2855.
(14) Joensen, P.; Frindt, R. F.; Morrison, S. R. Single-Layer MoS_2. *Mater. Res. Bull.* **1986**, *21*, 457−461.
(15) Divigalpitiya, W. M. R.; Frindt, R. F.; Morrison, S. R. Inclusion Systems of Organic Molecules in Restacked Single-Layer Molybdenum Disulfide. *Science* **1989**, *246*, 369−371.
(16) Ling, X.; Lee, Y.-H.; Lin, Y. X.; Fang, W. J.; Yu, L. L.; Dresselhaus, M. S.; Kong, J. Role of the Seeding Promoter in MoS_2 Growth by Chemical Vapor Deposition. *Nano Lett.* **2014**, *14*, 464−472.
(17) Yang, S. X.; Kang, J.; Yue, Q.; Yao, K. Vapor Phase Growth and Imaging Stacking Order of Bilayer Molybdenum Disulfide. *J. Phys. Chem. C* **2014**, *118*, 9203−9208.
(18) Liu, H.; Si, M. W.; Deng, Y. X.; Neal, A. T.; Du, Y. C.; Najmaei, S.; Ajayan, P. M.; Lou, J.; Ye, P. D. Switching Mechanism in Single-Layer Molybdenum Disulfide Transistors: An Insight into Current Flow across Schottky Barriers. *ACS Nano* **2014**, *8*, 1031−1038.
(19) Yu, Y. F.; Li, C.; Liu, Y.; Su, L. Q.; Zhang, Y.; Cao, L. Y. Controlled Scalable Synthesis of Uniform, High-Quality Monolayer and Few-Layer MoS_2 Films. *Sci. Rep.* **2013**, *3* (1866), 1−6.
(20) Park, W.; Baik, J.; Kim, T.-Y.; Cho, K.; Hong, W.-K.; Shin, H.-J.; Lee, T. Photoelectron Spectroscopic Imaging and Device Applications of Large-Area Patternable Single-Layer MoS_2 Synthesized by Chemical Vapor Deposition. *ACS Nano* **2014**, *8*, 4961−4968.
(21) Lauritsen, J. V.; Kibsgaard, J.; Helveg, S.; Topsøe, H.; Clausen, B. S.; Lægsgaard, E.; Besenbacher, F. Size-Dependent Structure of MoS_2 Nanocrystals. *Nat. Nanotechnol.* **2007**, *2*, 53−58.
(22) Peng, Y. Y.; Meng, Z. Y.; Zhong, C.; Lu, J.; Yu, W. C.; Jia, Y. B.; Qian, Y. T. Hydrothermal Synthesis and Characterization of Single-Molecular-Layer MoS_2 and $MoSe_2$. *Chem. Lett.* **2001**, *8*, 772−773.
(23) Tan, L. K.; Liu, B.; Teng, J. H.; Guo, S. F.; Low, H. Y.; Loh, K. P. Atomic Layer Deposition of a MoS_2 Film. *Nanoscale* **2014**, *6*, 10584−10588.
(24) Li, Q.; Newberg, J. T.; Walter, E. C.; Hemminger, J. C.; Penner, R. M. Polycrystalline Molybdenum Disulfide (2H-MoS_2) Nano- and Microribbons by Electrochemical/Chemical Synthesis. *Nano Lett.* **2004**, *4*, 277−281.
(25) Liu, K.-K.; Zhang, W. J.; Lee, Y.-H.; Lin, Y.-C.; Chang, M.-T.; Su, C.-Y.; Chang, C.-S.; Li, H.; Shi, Y. M.; Zhang, H.; Lai, C. S.; Li, L. J. Growth of Large-Area and Highly Crystalline MoS_2 Thin Layers on Insulating Substrates. *Nano Lett.* **2012**, *12*, 1538−1544.
(26) Lee, K.; Gatensby, R.; McEvoy, N.; Hallam, T.; Duesberg, G. S. High Performance Sensors Based on Molybdenum Disulfide Thin Films. *Adv. Mater.* **2013**, *25*, 6699−6702.
(27) Zhan, Y. J.; Liu, Z.; Najmaei, S.; Ajayan, P. M.; Lou, J. Large-Area Vapor-Phase Growth and Characterization of MoS_2 Atomic Layers on a SiO_2 Substrate. *Small* **2012**, *8*, 966−971.
(28) Lee, Y. B.; Lee, J.; Bark, H.; Oh, I.-K.; Ryu, G. H.; Lee, Z.; Kim, H.; Cho, J. H.; Ahn, J.-H.; Lee, C. G. Synthesis of Wafer-Scale Uniform Molybdenum Disulfide Films with Control over the Layer Number Using a Gas Phase Sulfur Precursor. *Nanoscale* **2014**, *6*, 2821−2826.
(29) Najmaei, S.; Liu, Z.; Zhou, W.; Zou, X. L.; Shi, G.; Lei, S. D.; Yakobson, B. I.; Idrobo, J.-C.; Ajayan, P. M.; Lou, J. Vapour Phase Growth and Grain Boundary Structure of Molybdenum Disulphide Atomic Layers. *Nat. Mater.* **2013**, *12*, 754−759.
(30) Lee, Y.-H.; Zhang, X.-Q.; Zhang, W. J.; Chang, M.-T.; Lin, C.-T.; Chang, K.-D.; Yu, Y.-C.; Wang, J. T.-W.; Chang, C.-S.; Li, L.-J.; Lin, T. W. Synthesis of Large-Area MoS_2 Atomic Layers with Chemical Vapor Deposition. *Adv. Mater.* **2012**, *24*, 2320−2325.
(31) Yin, Z. Y.; Zeng, Z. Y.; Liu, J. Q.; He, Q. Y.; Chen, P.; Zhang, H. Memory Devices Using a Mixture of MoS_2 and Graphene Oxide as the Active Layer. *Small* **2013**, *9*, 727−731.
(32) Li, X. L.; Li, Y. D. Formation of MoS_2 Inorganic Fullerenes (IFs) by the Reaction of MoO_3 Nanobelts and S. *Chem.—Eur. J.* **2003**, *9*, 2726−2731.
(33) Huang, J.-K.; Pu, J.; Hsu, C.-L.; Chiu, M.-H.; Juang, Z.-Y.; Chang, Y.-H.; Chang, W.-H.; Iwasa, Y.; Takenobu, T.; Li, L.-J. Large-Area Synthesis of Highly Crystalline WSe_2 Monolayers and Device Applications. *ACS Nano* **2014**, *8*, 923−930.
(34) Zhang, Y.; Zhang, Y. F.; Ji, Q. Q.; Ju, J.; Yuan, H. T.; Shi, J. P.; Gao, T.; Ma, D. L.; Liu, M. X.; Chen, Y. B.; Song, X. J.; Hwang, H. Y.; Cui, Y.; Liu, Z. F. Controlled Growth of High-Quality Monolayer WS_2 Layers on Sapphire and Imaging Its Grian Boundary. *ACS Nano* **2013**, *7*, 8963−8971.
(35) Shaw, J. C.; Zhou, H. L.; Chen, Y.; Weiss, N. O.; Liu, Y.; Huang, Y.; Duan, X. F. Chemical Vapor Deposition Growth of Monolayer $MoSe_2$ Nanosheets. *Nano Res.* **2014**, *7*, 511−517.
(36) van der Zande, A. M.; Huang, P. Y.; Chenet, D. A.; Berkelbach, T. C.; You, Y. M.; Lee, G.-H.; Heinz, T. F.; Reichman, D. R.; Muller, D. A.; Hone, J. C. Grains and Grain Boundaries in Highly Crystalline Monolayer Molybdenum Disulphide. *Nat. Mater.* **2013**, *12*, 554−561.
(37) Li, S.-L.; Miyazaki, H.; Song, H. S.; Kuramochi, H.; Nakaharai, S.; Tsukagoshi, K. Quantitative Raman Spectrum and Reliable Thickness Identification for Atomic Layers on Insulating Substrates. *ACS Nano* **2012**, *6*, 7381−7388.
(38) Eda, G.; Yamaguchi, H.; Voiry, D.; Fujita, T.; Chen, M. W.; Chhowalla, M. Photoluminescence from Chemically Exfoliated MoS_2. *Nano Lett.* **2011**, *11*, 5111−5116.
(39) Wypych, F.; Schöllhorn, R. 1T-MoS_2, a New Metallic Modification of Molybdenum Disulfide. *J. Chem. Soc., Chem. Commun.* **1992**, *19*, 1386−1388.
(40) Lai, K. J.; Peng, H. L.; Kundhikanjana, W.; Schoen, D. T.; Xie, C.; Meister, S.; Cui, Y.; Kelly, M. A.; Shen, Z.-X. Nanoscale Electronic Inhomogeneity in In_2Se_3 Nanoribbons Revealed by Microwave Impedance Microscopy. *Nano Lett.* **2009**, *9*, 1265−1269.
(41) Kasper, M. *Introduction to Scanning Microwave Microscopy Mode.* Application Note of Keysight Technologies, Inc., Publication No. 5989-8881EN, 2014.
(42) Tselev, A.; Lavrik, N. V.; Kolmakov, A.; Kalinin, S. V. Scanning Near-Field Microwave Microscopy of VO_2 and Chemical Vapor Deposition Graphene. *Adv. Funct. Mater.* **2013**, *23*, 2635−2645.
(43) Tselev, A.; Lavrik, N. V.; Vlassiouk, I.; Briggs, D. P.; Rutgers, M.; Proksch, R.; Kalinin, S. V. Near-Field Microwave Scanning Probe Imaging of Conductivity Inhomogeneities in CVD Graphene. *Nanotechnology* **2012**, *23*, 385706.

DOI: 10.1021/acsami.5b07038
ACS Appl. Mater. Interfaces 2015, 7, 22587−22593